Highly Fluorescent Metal-Organic-Framework Nanocomposites for Photonic Applications

A. Monguzzi[1], M. Ballabio[1], N. Yanai[2,3], N. Kimizuka[2], D. Fazzi[4], M. Campione[5], and F. Meinardi[1]**

[1]Dipartimento di Scienza dei Materiali, Università degli Studi Milano Bicocca via R. Cozzi 55, 20125 Milan , Italy

[2]Department of Chemistry and Biochemistry, Graduate School of Engineering, Center for Molecular Systems (CMS), Kyushu University, Moto-oka 744, Nishi-ku, Fukuoka-819-0395, Japan

[3]PRESTO, JST, Honcho 4-1-8, Kawaguchi, Saitama 332-0012, Japan

[4]Max-Planck-Institut für Kohlenforschung (MPI-KOFO) Kaiser-Wilhelm-Platz 1, D-45470 Mülheim an der Ruhr (Germany)

[5]Department of Earth and Environmental Sciences, Università degli Studi Milano-Bicocca, Piazza della Scienza 4, 20126 Milano, Italy.

KEYWORDS.
nanocrystals – excitons - metal-organic frameworks – nanocomposites – hybrid emitters

ABSTRACT

Metal-organic frameworks (MOFs) are porous hybrid materials built up from organic ligands coordinated to metal ions or clusters by means of self-assembly strategies. The peculiarity of these materials is the possibility, according to specific synthetic routes, to manipulate both the composition and ligands arrangement in order to control their optical and energy-transport properties. Therefore, optimized MOFs nanocrystals (nano-MOFs) can potentially represent the next generation of luminescent materials with features similar to those of their inorganic predecessors, i.e. the colloidal semiconductor quantum dots. The luminescence of fluorescent nano-MOFs is generated through the radiative recombination of ligand molecular excitons. The uniqueness of these nanocrystals is the possibility to pack the ligand chromophores close enough to allow a fast exciton diffusion but sufficiently far from each other preventing the aggregation-induced effects of the organic crystals. In particular, the formation of strongly coupled dimers or excimers is avoided, thus preserving the optical features of the isolated molecule. However, nano-MOFs have a very small fluorescence quantum yield (QY). In order to overcome this limitation and achieve highly emitting systems, we analyzed the fluorescence process in blue emitting nano-MOFs and modelled the diffusion and quenching mechanism of photogenerated singlet excitons. Our results demonstrate that the excitons quenching in nano-MOFs is mainly due to the presence of surface-located, non-radiative recombination centers. In analogy with their inorganic counterparts, we found that the passivation of the nano-MOF surfaces is a straightforward method to enhance the emission efficiency. By embedding the nanocrystals in an inert polymeric host we observed a +200% increment of the fluorescence QY, thus recovering the emission properties of the isolated ligand in solution.

Metal-organic frameworks (MOFs) are a large class of hybrid materials built up from organic molecules, so called ligands, which are coordinated to metal ions or clusters. These building blocks show remarkable self-assembly properties, which allow for the controlled growth of crystalline frameworks that can span in one, two or three dimensions.[1 2 3] The interest in these hybrid materials was born due to their tunable porosity, which makes MOFs the ideal candidates for industrial applications such as the gas storing and sensing. The research on this subject was very active in the last two decades, giving birth to a huge family of multifunctional materials.[4-11] Conversely, the work on luminescent MOFs has attracted much attention, [12 13 14, 15] but only recently the unceasing advances in this field lead to the development of MOF nanocrystals based on fluorescent ligands (nano-MOFs), which are a new class of intriguing optically active materials with tailored electronic properties for applications in photonics, optoelectronics and biomedicine.[7, 16-19] The key advantage of these nanomaterials is the possibility to design the material composition and the ligands arrangement in order to control their optical and energy-transport properties. This can lead, for example, to the fabrication of nanocrystals with highly anisotropic mobility for charges and excitons, which are able to collect the excitation energy into preferential active sites. This will make the nano-MOF an ideal light-harvester, paving the way for the realization of the long-time desired artificial photosynthesis.[12, 20, 21] On the other side, nano-MOFs are also excellent candidates to be used in light-emitting devices, due to their structural diversity and tunable emission. For these reasons, optimized MOFs nanocrystals can potentially represent the next generation of luminescent materials, with a tremendous impact similar to that one obtained by their inorganic predecessors, i. e. the colloidal semiconductor quantum dots.[22]

In nano-MOFs, the luminescence is generated through the radiative recombination of ligand molecular excitons. The peculiarity of these nanocrystals is the possibility to pack the

chromophores close enough to allow a fast exciton diffusion, but sufficiently far from each other preventing the aggregation phenomena common in organic crystals, such as the formation of strongly coupled dimers or excimers, preserving the isolated molecules optical features.[23, 24]. However, these nanocrystals have a poor fluorescence quantum yield (QY), as usually happens for larger luminescent MOFs.[13 25] This can be ascribed to the quenching of excitons before the radiative recombination that dissipates the largest part of the absorbed energy. With the aim to overcome this bottleneck, in this work we studied the fluorescence process in blue emitting nano-MOFs, introducing a model for the diffusion and quenching process of singlet excitons. Our results demonstrate that the excitons quenching in nano-MOFs can be ascribed mainly to the presence of surface-located, non-radiative recombination centres. In analogy with their inorganic counterparts,[26-28] the effective passivation of the nano-MOF surface by embedding in an inert polymeric host allows for a +200% increment of the fluorescence QY, [29] recovering the emission properties of the isolated ligand.

Figure 1 shows the structure of the nano-MOF employed. The ligand used to fabricate the hybrid nanocrystal is the *4,4'-(anthracene-9,10-diyl)dibenzoate* (ADB), a derivative of the *9,10-diphenylanthracene* (DPA). In ADB, the lateral phenyl rings are terminated with carboxylic groups that allow the anchoring to Zn^{2+} ions, in order to grow a self-assembled framework (Fig. 1a). The synthesis protocol is detailed in Experimental section of the Supporting Information. The phase

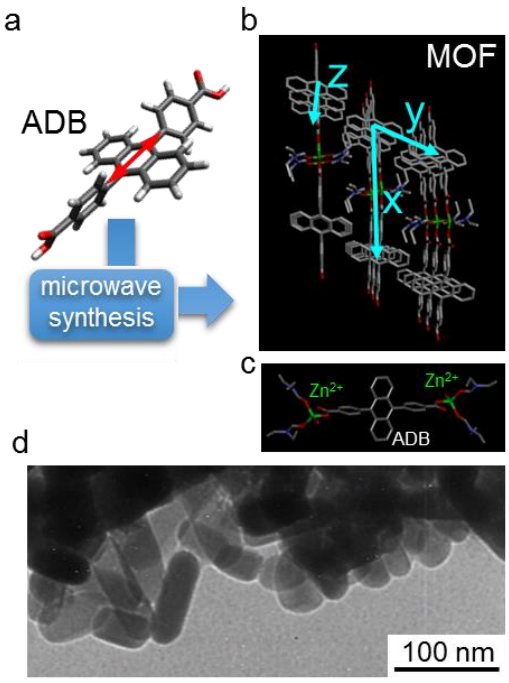

Figure 1. a) Molecular structure of the fluorescent ligand ADB employed to fabricate the metal-organic framework (MOF) nanocrystals by microwave synthesis. The red arrow depicts the orientation of the dipole moment for the $S_0 \leftrightarrow S_1$ electronic transition of the anthracene-like core. b) Crystalline lattice of the nano-MOF obtained from XRD analysis. The arrows indicate the directions considered for discussing the singlet excitons diffusion within the crystal framework. c) Detail of ADB-Zn^{2+} unit structure in the MOF framework. d) Transmission electron microscopy (TEM) image of bare nano-MOFs dropcasted from a benzene suspension.

purity of the nanocrystals was confirmed by elemental analysis and by the good agreement between the experimental and simulated x-ray powder diffraction (XRPD) patterns (Supporting Fig. S1). As like as for DPA, the ADB optical properties are determined by the conjugated anthracene core.[30] The transition dipole moment of the first allowed electronic transition $S_0 \leftrightarrow S_1$ is aligned with the short axis of the conjugated backbone (red arrow).[31] The ADB, in solution of dimethylformamide, absorbs in the near-UV region and shows a blue PL peaked at 2.85 eV, with a fluorescence lifetime of $\tau_{ADB} = 5.3$ ns. By considering the natural recombination time of $\tau_{rad} = 6.4$ ns, obtained from absorption/PL data using the Strickler-Berg equation, we calculated the

fluorescence quantum yield at room temperature using QY = (τ_{ADB} / τ_{rad}) = 0.81 (see Supporting Information and Fig. S2). Figs. 1b and 1c show the nano-MOF crystalline structure obtained by the XRPD analysis. The Zn^{2+} ions are connected by ADB ligands to form one-dimensional chains, with a closest center-to-center distance between the anthracene cores ~9.0 Å. The transmission electron microscopy (TEM) image reported in Fig. 1d shows that the nanocrystals have a pretty regular elongated shape, with a maximum length of ~100 nm.

The left panel of Figure 2a sketches the fundamental photophysical processes occurring upon singlets photo-excitation in the nano-MOF. After their generation upon the absorption of a UV photon, singlet excitons in the nanocrystal can randomly displace for each allowed crystallographic direction i by an average distance L_i, which is determined by their spontaneous lifetime τ_0 and diffusivity D_i through [24, 32]

$$L_i = \sqrt{2D_i\tau_0}. \qquad (1)$$

If this singlet diffusion length L_i is large enough to reach a non-radiative recombination centre (trap) before the natural decay, the excitons are quenched, with a consequent reduction of QY in respect to that one in solution. This phenomenon is rather common in organic crystalline solids, in which the presence of structural defects and/or impurities is an unavoidable loss channel because of the large excitons diffusivities.[33 34] This detrimental effect is even more relevant for nano-sized systems where the surface-to-volume ratio is very large, as surfaces and interfaces have different electronic properties in respect to the bulk and, in general, they behave as preferential trap sites for excitons and charges.[35]

The analysis of our nano-MOFs PL properties, by means of continuous-wave and time-resolved optical spectroscopy measurements, indicates that the scenario described above is fully valid. The PL excitation (PLE) spectrum of nanocrystals in benzene suspension is identical to that

one of the isolated ligand in solution (Fig. 2b and Fig. S2), showing the same vibronic replica series. This demonstrates that the controlled packing of constituting chromophores avoids strong intermolecular interactions which would results in an optical behavior critically different from that of the isolated molecules.[24] The PL spectrum of the nano-MOFs is similar to that of the isolated ligands, showing only a small red-shift (ΔE = 90 meV) that suggests the presence of a distribution of emitting states with energies lower than the S_1 state of the isolated ligand contributing to the overall emission. The time-resolved PL data show a peculiar exciton decay kinetic in nano-MOFs, which is dominated by the occurrence of competitive non-radiative recombination channels. The signal decay is multi-exponential, as expected for migration-mediated energy quenching by a defects distribution and its decay time is as short as τ = 1.5 ns, i.e. more than three times faster than that of ADB in solution (τ = 5.3 ns), with a consequent reduction of the QY down to 0.24 (Fig. 2d). Importantly, the cooling of the crystals down to 77 K does not extend significantly the PL lifetime giving only a small increment of the QY to 0.35, quite far from the emission efficiency of the isolated ADB. This weak dependence on the temperature of the PL lifetime demonstrates that, as like as for ADB, the intra-molecular vibrational relaxations does not limit significantly the nano-MOFs fluorescence (Fig. S2). On the contrary, it suggests once more that the major responsible of the singlet excitons quenching is their fast migration towards energetic traps.

In general, exciton traps may be found both in the bulk of the crystal and at the surface. The removal of bulk defects/impurities is not an easy task, because their amount and distribution can be controlled only during the synthesis route. On the other hand, the surface, thanks to its natural interaction with the surrounding environment, is suitable for functionalization or chemically treatments *a posteriori*. It is worth pointing out that this synthetic approach lead to the development of high performance semiconductor nanocrystals with PL yields close to 100%,

thanks to an accurate and targeted engineering of their surfaces.[28, 36-39] In order to extend this strategy to nano-MOFs, by taking inspiration from previous works, [40, 41] we embedded the nanocrystals in an optically inert polymer able to passivate the traps on the crystal surfaces and therefore to enhance the QY, as schematically illustrated in the right panel of Fig. 2a.[33, 42] To this aim, we used the poly(methylmethacrylate) (PMMA), which is a well known plastic material with excellent structural properties and high transparency in the near UV-Vis spectral range. It is also easy to handle by countless synthetic procedures, and widely used for research and industrial applications.[43] The nano-MOF:PMMA composite film has been prepared by dispersing the nanocrystals powder in a toluene:PMMA solution, which has been successively drop-casted as a thin film on a glass substrate to allow the solvent evaporation (see Supporting Information). Considered the large excess of PMMA in respect to the nanocrystals and given the chemical affinity of the PMMA with the MOF organic component, whose interaction can be favoured by the formation of H-bonds between the carboxylic moiety of ADB and the acrylic moiety of PMMA, we speculate that the polymer can shell the embedded nanocrystals by saturating the dangling bonds due under-coordinated ligands or metal ions on the crystal surfaces.[44] The effects of this embedding on the nanocrystal fluorescence are shown in Fig. 2c. The PLE is not modified by the polymer shell, as expected considering that the light absorption is a typical bulk process. On the contrary, striking differences appear in the PL shape and lifetime in respect to the system in suspension. Now, a structured shape is detectable also in the emission spectrum and it does not show any red-shift in respect to the ligand PL. This suggests the successful removal of the surface-related emitting centres responsible for the red-shift of the luminescence in unprotected nano-MOFs, and of their PL quenching. Accordingly, the PL lifetime is extended to 4.6 ns, which

corresponds to a QY increase up to 0.72 (Fig. 2d). This finding is further confirmed by the direct measurement of QYs

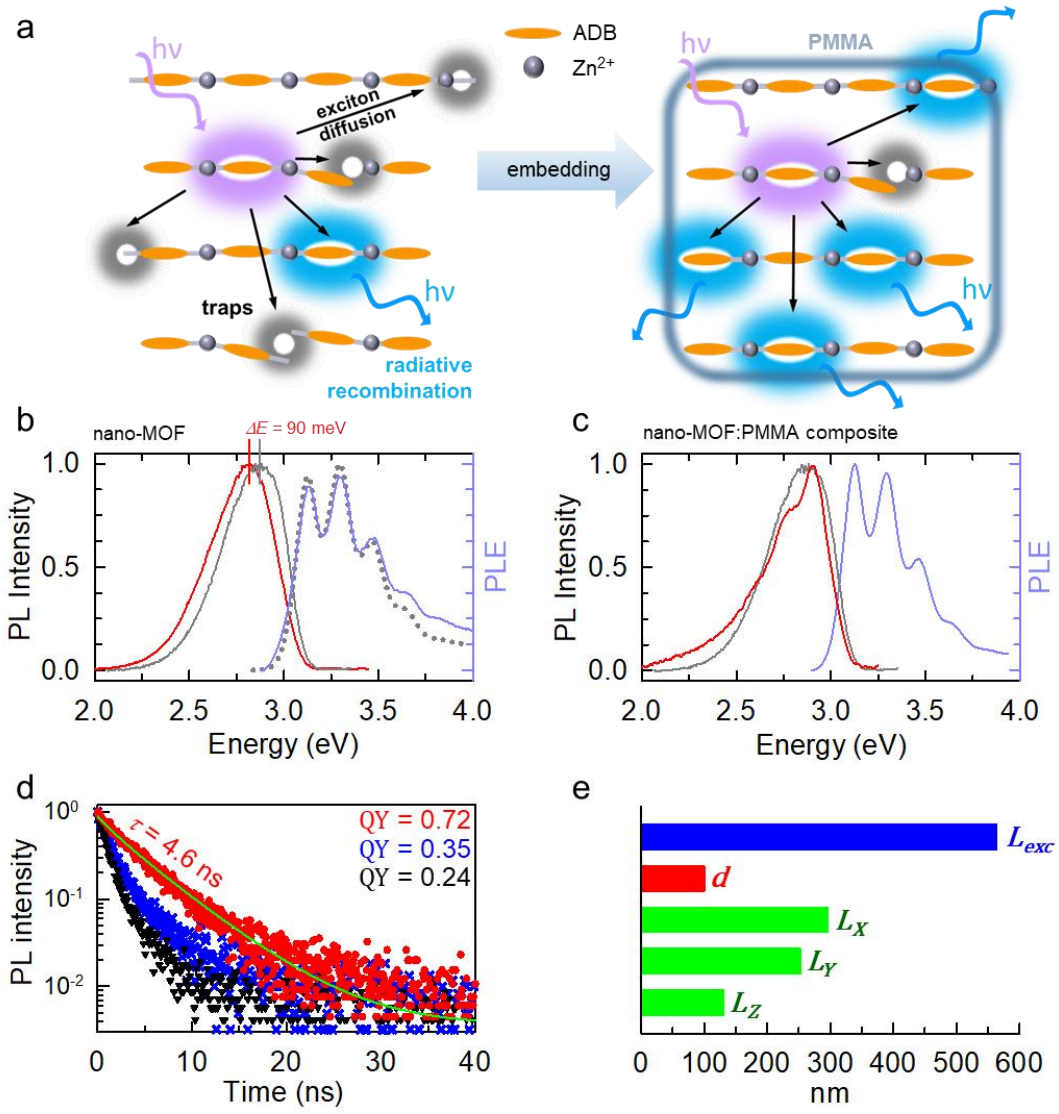

Figure 2. a) Sketch of the excitation, diffusion, radiative recombination and quenching processes for the singlet exciton in a fluorescent ligand-based MOF nanocrystal (left panel). The passivation of the surface by encapsulation in a polymeric shell reduces the singlets quenching leading to an increment of the emission yield (right panel). b, c) PL and PL excitation (PLE) spectra of a nano-MOF suspension in benzene (b), and of the nano-MOF:PMMA composite (c). The ADB ligand PLE (dotted line) and PL spectrum in solution (grey line) are reported for comparison. d) Time-resolved PL decays of nano-MOFs in benzene at room temperature (triangles) and 77 K (crosses) compared to the PL decay of nano-MOFs:PMMA (dots). The solid line is the fit of data with a stretched exponential decay function. The PLs have a characteristic lifetime of 1.5 ns, 2.2 ns and 4.6 ns, which corresponds to an emission quantum yield of 0.24, 0.35 and 0.72, respectively. e) Comparison between the excitation light penetration depth L_{exc}, the largest crystal dimension d and the calculated exciton diffusion lengths L_i along the direction indicated in Fig. 1b (i = x, y, z).

with relative and absolute methods (Supporting Tab. 1). We notice that, even if the main PL overlaps very well the ligand emission shape, there is a weak emission contribution around 2.2-2.4 eV, which is not recognizable in the corresponding suspension. Its lifetime is considerably longer than the lifetime of the main emission (Fig. S6), which suggests that it originates from non-intrinsic emitting centers. We tentatively ascribe this side emission to new surface states induced by the PMMA encapsulation or, eventually, to bulk defects. In the latter case, their PL is not detectable before the embedding procedure because the surface traps are more effective in the exciton capture.

The results obtained hint that the excited singlet quenching in nano-MOFs can be ascribed to surfaces defects rather than to traps that localized in the nanocrystal volume, even if their nature is stil debated. For example, they have been ascribed to a different aggregation structure probably due to intrinsic metal vacancies as well as to surface reconstruction.[45] Regardelss their specific origin, in order to further point out their key role in the quenching of the nano-MOFs fluorescence, we analyze in detail the exciton generation and diffusion processes. As far as the distribution of photo-generated excitons inside the nano-MOF is concerned, by knowing the oscillator strength of the ADB $S_0 \leftrightarrow S_1$ electronic transition and the number of chromophores per cubic centimeter, it is possible to calculate the penetration depth L_{exc} of the excitation light (see Supplementary Information).[24] In our case L_{exc} = 564 nm, which is a distance almost six times larger than the longest axis of the nanocrystals ($d \sim$ 100 nm, Fig. 1c). Therefore, it is reasonable to assume that excited singlets are generated uniformly in the whole volume of the nano-MOFs, and not only in the first molecular layers close to the crystal surface where the quenching rate should be especially large, even in the case of low-mobility molecular excitons. For this reason, it is particularly

important to evaluate the excited state diffusion length L because only if $L/d >> 1$ the excitons are almost free to move within the whole nano-MOF volume before the recombination. Conversely, if $L/d << 1$ the excitons generated in the inner part of the crystal remains localized, and consequently they are expected to be insensitive to any sort of surface-related phenomena. Since the crystals structure of our nano-MOFs is highly anisotropic, L_i have been calculated using Eq. 1 for the three crystallographic directions i = x, y, z showed in Fig. 1b. For the evaluation of the three diffusion coefficients D_i, we assumed that singlets travel within the nanocrystal *via* homo-molecular hopping driven by Förster resonant energy transfer (FRET) through the ligand network.[32] The FRET is based on a dipole–dipole electromagnetic approximation,[46] and therefore it implicitly introduces an underestimation of the transfer rates and diffusivities by neglecting other interaction terms such as the exchange contributions, as derived in the formal equation of the exciton coupling matrix terms, [47] and the through-bond Coulombic contributions via the metal centers, here present in the nano-MOFs. However, this approximation is reasonable considering that FRET usually outperforms the efficiency of the exchange-driven transfer for singlets in solids where the inter-molecular distances are comparable to chromophores dimensions.[32] [48] To support our general model, we performed a quantum-mechanical modelling of the singlet excitons coupling in the nano-MOF adopting linear-response time dependent density functional theory (TDDFT) and semiempirical (ZINDO/S) approaches. As detailed in the Supporting Tab. 4, the exciton coupling between nearest-neighbors chromophores in the nano-MOF has been computed by using the so-called supermolecular approach, resulting of the order of tens meV. [49] It is worth pointing out that these values are typical of weak interacting molecules, further corroborating the experimental observation, i.e. the nanocrystal optical properties are similar to those of the isolated ligand. This finding justifies our hypothesis that the molecular exciton generated on a given ligand

moves successively within the emitter framework. The coupling with the next nearest-neighbor dyes (i.e. second, third, etc.) is significantly lower (Fig. S5), as expected when short range interactions are vanishing. This latter result excludes that the singlet long-range diffusion in the nano-MOF is driven by exchange-mediated hopping, indicating that it relies mainly on FRET mechanism based on long-range coulombic interactions.[50]

Once verified that the nano-MOF ligands can be effectively considered as isolated chromophores, we estimated the hopping rate k_{hop} of the singlet exciton directly from experimental data using

$$k_{hop} = k_{Fs} = k_D \left(\frac{R}{R_0}\right)^6, \quad (2)$$

where k_{Fs} is the Förster ET rate, $k_D = (\tau_{ADB})^{-1}$ is the energy donor excited state decay rate in absence of the energy acceptor, R is the donor/acceptor inter-molecular distance and R_0 are the Förster radii in the different directions that depend from the overlap between the emission/absorption spectra and from the relative orientations between the transition dipole moment of the involved molecules.[51] It should be noted that, considering the structural data reported in the Supporting Tab. 3 and that the transition dipole length of the MOF ligand showed in Fig. 1a, the Eq. 2 is strictly valid in the point-dipole approximation of the classic Förster model, i.e when R is larger than the length of the transition dipole moment involved.[52] The obtained values for R_0, and k_{hop}, reported in the Supporting Information, have been calculated by using as k_D the radiative decay rate of an isolated ADB molecule which represents the bottom limit for this rate. Considering that the diffusivity is given by [53, 54]

$$D_i = \left(k_{hop} R^2\right)_i, \quad (3)$$

we calculated the mono-dimensional diffusion length along each crystalline direction, as reported in Fig. 2e. Notably, these lengths (L_i = 296 nm, 252 nm, and 131 nm along x, y and z, respectively),

are larger than the nanocrystal maximum size d. This result points out that, independently from the exact point in which the excitons are generated, they can explore the whole crystal during their lifetime, thus resulting prone to surface traps quenching. This result explains why the surface passivation by encapsulation in PMMA induces the remarkable three times enhancement of the QY. The residual difference in the emission yield between the nanocomposite and the isolated ligand (~11%) is probably due to bulk traps which, even if present in a concentration much smaller than the surface defects, can still act as secondary energy dissipation channels.

In order to demonstrate the general validity of our approach, we repeated the whole experiment with other nano-sized MOFs, fabricated using the same fluorescent ligands but arranged in different lattices. Figure 3 reports the XRD data and the TEM images for two alternative nanocrystals obtained using the ADB in presence with two different co-ligands, namely *4,4'-bipiridine* (MOF-bpy) (Fig. 3a) and *1,4-diazabicyclo[2.2.2]octane* (MOF-dabco) (Fig. 3d) [55], which are optically inert and commonly used as MOF building blocks.[56] [57] Despite the structural analysis shows that these latter nanoscale MOFs are different in both structure and size of the crystal in respect to the first case (Fig 3b, d), their PL and PLE (Fig 3c, f) spectra show again the features of the ligand, with low QYs in suspension. Remarkably, when protected in a plastic PMMA matrices also the QY of this nanocrystals rises from ~ 0.25 to 0.70 and 0.58 for MOF-bpy and MOF-dabco, respectively. It is interesting to observe that the benefits of the encapsulation are less evident for the MOF-dabco in respect to the other two systems. This difference can be explained by correlating the nanocrystals L/d ratio and the QY rise. The MOF-dabco is the only one in which the average crystal size is larger than the diffusion length in all directions (Fig. 3e). Therefore, while in the other two MOFs the excited singlets can explore the entire nanocrystal, in the MOF-dabco the excitons generated in the inner volume do not reach the surface. Consequently,

these relatively large crystals, characterized by a reduced surface-to-volume ratio, result less sensitive to surface treatments aimed to remove the fluorescence-quenching sites located at the

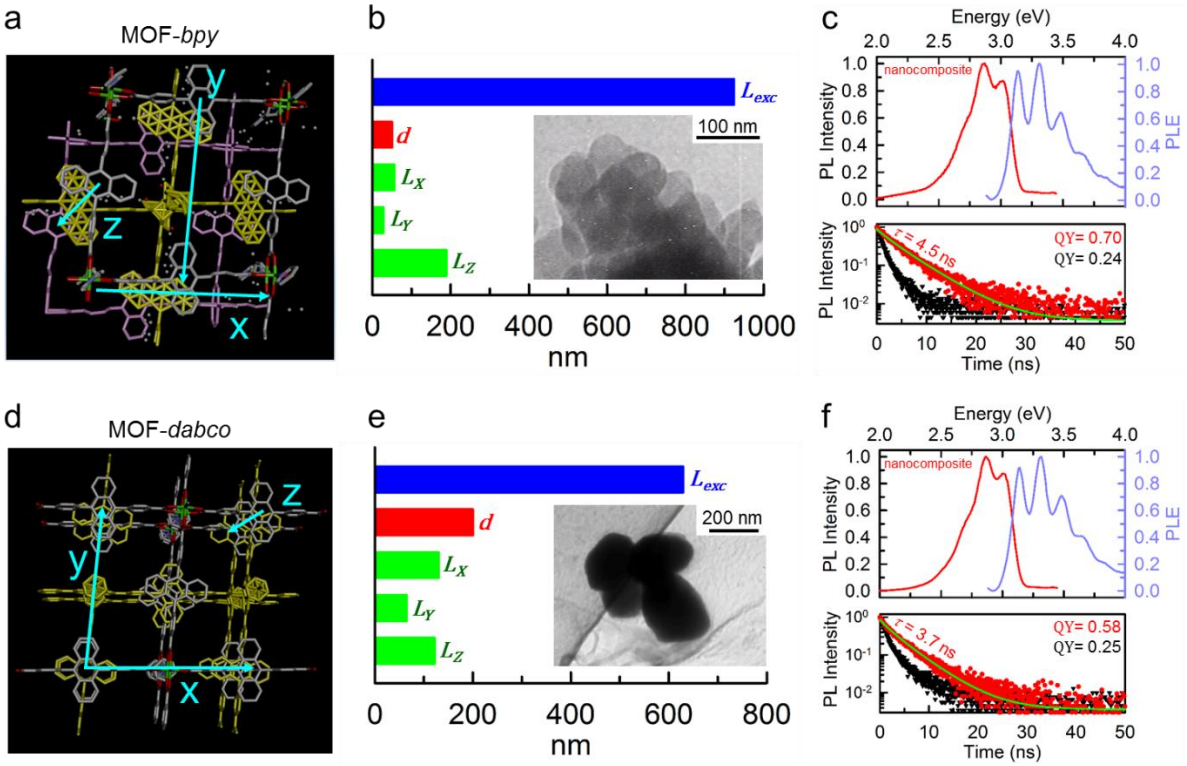

Figure 3. a, d) Crystalline lattice of two additional fluorescent nano-MOFs (MOF-*bpy*, MOF-*dabco*) obtained by using ADB as ligand. The arrows indicate the direction considered for discussing the singlet excitons diffusion within the crystalline lattice. b, e) Comparison between L_{exc}, d and the calculated exciton diffusion lengths L_i along the direction indicated in Fig. 3a, d. The inset reports a TEM image of the bare nanocrystals. c, f) PL, PLE and time-resolved luminescence spectra of MOF-*bpy*, MOF-*dabco* nanocomposites in PMMA. The triangles show the PL decay for bare nanocrystals in benzene suspension.

interface. As a consequence, their photoluminescence QY is mainly controlled by the presence of intrinsic bulk defects and impurities. This picture is further confirmed by comparing the data collected for different sizes of the same nano-MOF. In particular, we synthesized MOF-dabco nanocrystals with an average size of ~500 nm, which is about two times larger than that one of the previous batch. In this case, the singlets diffusion lengths are shorter that the average crystal size.

In agreement with the proposed key role of the surface trap states, these new MOFs in benzene suspension show a photoluminescence QY as high as 0.36, i. e. 1.5 times larger than the QY of the smaller ones. Correspondingly, because in this case the surface traps are not the main exciton quenching channel, the embedding of these nano-MOFs in PMMA give rise to only a small increment of the QY up to 0.47 (Fig. S7).

In conclusion, we have demonstrated that the emission efficiency of MOF nanocrystals is controlled by surface traps that introduce non-radiative recombination channels, unless the MOF dimensions exceed the exciton diffusion length. However, as in the case of semiconductor colloidal quantum dots, a proper passivation of the MOF surface allows us to rise their photoluminescence QY which approaches the same value of the emitter employed as ligand. In particular we obtained highly emissive MOF trough their embedding in a PMMA matrix with the additional results of obtaining a nanocomposite based on a processable, stable, cost effective and versatile polymer, which is compatible with many industrial processes for device fabrication such as the multilayer thin film deposition, roll-to-roll printing and bulk polymerization. These findings completely change the current vision of the MOF as a system not particularly suitable for optical applications, and pave the way for future works aimed to the development of a next generation of multifunctional photonic devices for lighting and photon managing applications, for example in luminescent solar concentrators,[58] based on non-toxic hybrid materials. It is worth pointing out that the proposed strategy can be extended in principle to other systems as conductive polymers, in order to realize optolectronic devices, and advanced polymerization techinques can be employed to obtain dispersible encapsulated highly luminescent nanocrystals.[59]

ASSOCIATED CONTENT

Supporting Information.

Experimental methods, additional data and figures that support the structural and optical characterization of the MOF nanocrystals, together with the details on the diffusion lengths calculation and the quantum-mechanical modeling employed.

AUTHOR INFORMATION

Corresponding Authors

* Email: angelo.monguzzi@unimib.it
* Email: franco.meinardi@mater.unimib.it

Author Contributions

The manuscript was written through contributions of all authors. All authors have given approval to the final version of the manuscript.

Notes

The authors declare no competing financial interest.

ACKNOWLEDGMENT

A. M. acknowledges support from Università degli Studi Milano-Bicocca (grant n°2016-ATESP-0052) and Fondazione Cariplo (grant n°2016-0925 IRIS:2016-NAZ-0050)

REFERENCES

(1) Yaghi, O. M.; O'Keeffe, M.; Ockwig, N. W.; Chae, H. K.; Eddaoudi, M.; Kim, J. *Nature* **2003,** 423, 705-714.
(2) Kitagawa, S.; Kitaura, R.; Noro, S. *Angew. Chem. Int. Ed.* **2004,** 43, 2334-75.
(3) Ferey, G.; Serre, C. *Chem. Soc. Rev.* **2009,** 38, 1380-1399.
(4) Li, J. R.; Sculley, J.; Zhou, H. C. *Chem. Rev.* **2012,** 112, 869-932.
(5) Yamada, T.; Otsubo, K.; Makiura, R.; Kitagawa, H. *Chem. Soc. Rev.* **2013,** 42, 6655-6669.
(6) Sun, L.; Campbell, M. G.; Dincă, M. *Angew. Chem. Int. Ed.* **2016,** 55, 3566-3579.
(7) Evans, J. D.; Sumby, C. J.; Doonan, C. J. *Chem. Soc. Rev.* **2014,** 43, 5933-5951.
(8) Suh, M. P.; Park, H. J.; Prasad, T. K.; Lim, D.-W. *Chem. Rev.* **2012,** 112, 782-835.
(9) Sindoro, M.; Yanai, N.; Jee, A.-Y.; Granick, S. *Acc. Chem. Res.* **2014,** 47, 459-469.
(10) Yanai, N.; Kitayama, K.; Hijikata, Y.; Sato, H.; Matsuda, R.; Kubota, Y.; Takata, M.; Mizuno, M.; Uemura, T.; Kitagawa, S. *Nat. Mater.* **2011,** 10, 787-793.
(11) Distefano, G.; Suzuki, H.; Tsujimoto, M.; Isoda, S.; Bracco, S.; Comotti, A.; Sozzani, P.; Uemura, T.; Kitagawa, S. *Nat. Chem.* **2013,** 5, 335-341.
(12) Zhang, T.; Lin, W. *Chem. Soc. Rev.* **2014,** 43, 5982-5993.
(13) Allendorf, M. D.; Bauer, C. A.; Bhakta, R. K.; Houk, R. J. T. *Chem. Soc. Rev.* **2009,** 38, 1330-1352.
(14) So, M. C.; Wiederrecht, G. P.; Mondloch, J. E.; Hupp, J. T.; Farha, O. K. *Chem. Commun.* **2015,** 51, 3501-3510.
(15) Cui, Y.; Yue, Y.; Qian, G.; Chen, B. *Chem. Rev.* **2012,** 112, 1126-1162.
(16) Nagarkar, S. S.; Saha, T.; Desai, A. V.; Talukdar, P.; Ghosh, S. K. *Sci. Rep.* **2014,** 4, 7053.
(17) Suresh, V. M.; George, S. J.; Maji, T. K. *Adv. Funct. Mater.* **2013,** 23, 5585-5590.
(18) White, K. A.; Chengelis, D. A.; Gogick, K. A.; Stehman, J.; Rosi, N. L.; Petoud, S. *J. Am. Chem. Soc.* **2009,** 131, 18069-18071.
(19) Kent, C. A.; Liu, D.; Ma, L.; Papanikolas, J. M.; Meyer, T. J.; Lin, W. *J. Am. Chem. Soc.* **2011,** 133, 12940-12943.
(20) Abe, K.; Zhao, L.; Periasamy, A.; Intes, X.; Barroso, M. *PLoS ONE* **2013,** 8, e80269.
(21) Sholl, D. S.; Lively, R. P. *J. Phys. Chem. Lett.* **2015,** 6, 3437-3444.
(22) Pietryga, J. M.; Park, Y.-S.; Lim, J.; Fidler, A. F.; Bae, W. K.; Brovelli, S.; Klimov, V. I. *Chem. Rev.* **2016,** 116, 10513-10622.
(23) Hunter, C. A.; Sanders, J. K. M.; Stone, A. J. *Chem. Phys.* **1989,** 133, 395-404.
(24) Pope, M.; Swenberg, C. E.; Pope, M., *Electronic processes in organic crystals and polymers*. Oxford University Press: New York, 1999.
(25) Bauer, C. A.; Timofeeva, T. V.; Settersten, T. B.; Patterson, B. D.; Liu, V. H.; Simmons, B. A.; Allendorf, M. D. *J. Am. Chem. Soc.* **2007,** 129, 7136-7144.
(26) Wang, X.-S.; Dykstra, T. E.; Salvador, M. R.; Manners, I.; Scholes, G. D.; Winnik, M. A. *J. Am. Chem. Soc.* **2004,** 126, 7784-7785.
(27) Park, H. W.; Kim, D.-H. *J. Nanomat.* **2012,** 2012, 6.
(28) Wei, H. H.-Y.; Evans, C. M.; Swartz, B. D.; Neukirch, A. J.; Young, J.; Prezhdo, O. V.; Krauss, T. D. *Nano Lett.* **2012,** 12, 4465-4471.
(29) Tamborra, M.; Striccoli, M.; Comparelli, R.; Curri, M. L.; Petrella, A.; Agostiano, A. *Nanotechnology* **2004,** 15, S240.

(30) Morris, J. V.; Mahaney, M. A.; Huber, J. R. *J. Phys. Chem.* **1976,** 80, 969-974.
(31) Quarti, C.; Fazzi, D.; Del Zoppo, M. *Phys. Chem. Chem. Phys.* **2011,** 13, 18615-18625.
(32) Mikhnenko, O. V.; Blom, P. W. M.; Nguyen, T.-Q. *Energ. Environ. Sci.* **2015,** 8, 1867-1888.
(33) Gierschner, J.; Lüer, L.; Milián-Medina, B.; Oelkrug, D.; Egelhaaf, H.-J. *J. Phys. Chem. Lett.* **2013,** 4, 2686-2697.
(34) Zatryb, G.; Podhorodecki, A.; Misiewicz, J.; Cardin, J.; Gourbilleau, F. *Nanosc. Res. Lett.* **2011,** 6, 1-8.
(35) Schlegel, G.; Bohnenberger, J.; Potapova, I.; Mews, A. *Phys. Rev. Lett.* **2002,** 88, 137401.
(36) Yuan, M.; Liu, M.; Sargent, E. H. *Nat. Energ.* **2016,** 1, 16016.
(37) Gaponik, N.; Talapin, D. V.; Rogach, A. L.; Hoppe, K.; Shevchenko, E. V.; Kornowski, A.; Eychmüller, A.; Weller, H. *J. Phys. Chem. B* **2002,** 106, 7177-7185.
(38) Talapin, D. V.; Rogach, A. L.; Kornowski, A.; Haase, M.; Weller, H. *Nano Lett.* **2001,** 1, 207-211.
(39) Bao, H.; Gong, Y.; Li, Z.; Gao, M. *Chem. Mater.* **2004,** 16, 3853-3859.
(40) Fery-Forgues, S. *Nanoscale* **2013,** 5, 8428-8442.
(41) Philippot, C.; Dubois, F.; Maurin, M.; Boury, B.; Prat, A.; Ibanez, A. *J. Mater. Chem.* **2012,** 22, 11370-11378.
(42) Wang, X.; Xu, S.; Xu, W. *Phys. Chem. Chem. Phys.* **2011,** 13, 1560-1567.
(43) Ali, U.; Karim, K. J. B. A.; Buang, N. A. *Polym. Rev.* **2015,** 55, 678-705.
(44) Kilina, S. V.; Tamukong, P. K.; Kilin, D. S. *Acc. Chem. Res.* **2016,** 49, 2127-2135.
(45) Fang, Z.; Bueken, B.; De Vos, D. E.; Fischer, R. A. *Angew. Chem. Int. Ed.* **2015,** 54, 7234-7254.
(46) Mirkovic, T.; Ostroumov, E. E.; Anna, J. M.; van Grondelle, R.; Govindjee; Scholes, G. D. *Chem. Rev.* **2017,** 117, 249-293.
(47) Scholes, G. D.; Ghiggino, K. P. *J. Phys. Chem.* **1994,** 98, 4580-4590.
(48) Scholes, G. D. *Annu. Rev. Phys. Chem.* **2003,** 54, 57-87.
(49) Brédas, J.-L.; Beljonne, D.; Coropceanu, V.; Cornil, J. *Chem.* **2004,** 104, 4971-5004.
(50) Zhang, Q.; Zhang, C.; Cao, L.; Wang, Z.; An, B.; Lin, Z.; Huang, R.; Zhang, Z.; Wang, C.; Lin, W. *J. Am. Chem. Soc.* **2016,** 138, 5308-5315.
(51) Lakowicz, J. R., *Principles of fluorescence spectroscopy*. Springer: New York, 2006.
(52) Förster, T. *Ann. der Physik* **1948,** 437, 55-75.
(53) Einstein, A. *Ann. der Physik* **1905,** 17, 549.
(54) Von Smoluchowski, M. *Ann. der physik* **1906,** 326, 756-780.
(55) Hauptvogel, I. M.; Biedermann, R.; Klein, N.; Senkovska, I.; Cadiau, A.; Wallacher, D.; Feyerherm, R.; Kaskel, S. *Inorg. Chem.* **2011,** 50, 8367-8374.
(56) Ohmura, T.; Usuki, A.; Mukae, Y.; Motegi, H.; Kajiya, S.; Yamamoto, M.; Senda, S.; Matsumoto, T.; Tatsumi, K. *Chemistry – An Asian Journal* **2016,** 11, (5), 700-704.
(57) Kitagawa, S.; Kitaura, R.; Noro, S.-i. *Angew. Chem. Int. Ed.* **2004,** 43, 2334-2375.
(58) Meinardi, F.; Ehrenberg, S.; Dhamo, L.; Carulli, F.; Mauri, M.; Bruni, F.; Simonutti, R.; Kortshagen, U.; Brovelli, S. *Nat. Photon.* **2017,** 11, 177-185.
(59) Li, K.; Liu, B. *Chem. Soc. Rev.* **2014,** 43, 6570-6597.

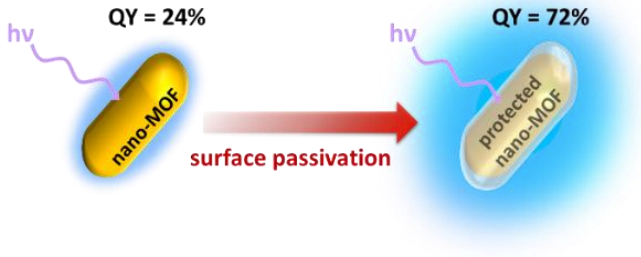
QY = 24%
hv
nano-MOF
surface passivation
QY = 72%
hv
protected
nano-MOF